Single Molecule Spectroscopy Studies of Diffusion in Mesoporous Silica Thin Films

Yi Fu,[‡] Fangmao Ye, William G. Sanders, Maryanne M. Collinson,*[,†] and Daniel A. Higgins*

Department of Chemistry, Kansas State University, Manhattan, Kansas 66506

Received: July 28, 2005; In Final Form: February 1, 2006

Single molecule spectroscopy is applied in studies of diffusion and surface adsorption in sol−gel-derived mesoporous silica thin films. Mesoporous films are obtained by spin casting surfactant-templated sols onto glass substrates. Small-angle X-ray diffraction results are consistent with hexagonally ordered mesophases in as-synthesized (i.e., surfactant-containing) films. Upon calcination, a 30% contraction and disordering of these structures occurs. Nile Red is used as a fluorescent probe of both the as-synthesized and calcined films. It is loaded into the samples at subnanomolar levels either prior to spin casting or after calcination. Fluorescence imaging and single-point fluorescence time transients show the dye molecules to be relatively mobile in the as-synthesized samples. In contrast, the molecules appear entrapped at fixed locations in dry calcined films. In calcined films rehydrated under high humidity conditions, the Nile Red molecules again become mobile. Time transients obtained from the as-synthesized and rehydrated samples provide clear evidence for frequent reversible adsorption of the dye to the silica surfaces. Autocorrelations of the time transients provide quantitative data on the mean diffusion coefficients ($D = 2.4 \times 10^{-10}$ and 2.6×10^{-10} cm^2/s) and mean desorption times ($1/k = 25$ and 40 s) for the as-synthesized and rehydrated films, respectively. The results prove both water and surfactant play important roles in governing matrix interactions and mass transport.

Introduction

Mesoporous silica materials prepared by templating silica sols with surfactant assemblies have attracted considerable interest since their discovery more than a decade ago.[1,2] Although once limited to powders and monoliths, the preparation of mesoporous thin films incorporating hexagonal, lamellar, and/or cubic mesophases by either dip coating or spin coating a templated sol onto a suitable substrate is now routine.[3−13] Mesoporous silica films have many advantages over more thoroughly studied "disordered" sol−gel-derived films.[14] These include long-range order, tunable pore size, and narrow pore size distributions. Their surfaces can also be easily modified with specific functional groups[15−17] and they can be loaded with analytical reagents (i.e., dyes)[9−11,18−20] via postsynthesis or in situ procedures.

Dye-doped mesoporous materials have numerous applications in the areas of pH sensing,[20] photochromism,[21] solid-state lasers,[22−24] and waveguide assemblies.[23] Of utmost importance to these applications are the mobility of the entrapped dye, its location, and the frequency and strength of its interactions with the pore surfaces, all of which play a profound role in governing ultimate device performance characteristics. Bulk fluorescence spectroscopy has long been used to obtain an average picture of these and other relevant materials properties.[25] For example, the formation of mesoporous thin films during dip coating has been probed by fluorescence methods.[10,11,26] Fluorescence spectroscopy has also been used to characterize the location, accessibility, and interactions of entrapped dyes.[27,28] Unfortunately, the underlying single particle motions and rare events associated with the detailed mechanism(s) of mass transport and molecule−matrix interactions are masked in such bulk experiments.

In this paper, single molecule fluorescence imaging and spectroscopy[29−31] are used to study the mass transport and matrix interactions of Nile Red trapped in mesoporous silica thin films of predominately hexagonal order. As-synthesized and calcined materials (both dry and rehydrated) are studied. Single molecule fluorescence correlation spectroscopy (FCS) methods are employed to measure the Nile Red diffusion coefficient and the length of adsorption events in nanoscale sample regions. FCS methods[32] have previously allowed for the characterization of single molecule Brownian motion[33−35] and rare strong adsorption events[34−36] in related materials. FCS methods and single particle tracking[37] have also been applied to the study of such phenomena in commercial and monolithic ordered mesoporous materials by the Dai group[36] and by Brauchle and co-workers.[38] Related studies of disordered mesoporous films have been reported by the Harris group.[39] While much was learned in these earlier studies, they dealt with fundamentally different materials (some were monoliths) that were prepared by different methods. It is particularly noteworthy that monoliths and thin film mesoporous materials are expected to have different properties in part because of differences in the rates at which hydrolysis, condensation, and solvent evaporation occur. Much work remains to be done to fully understand the dynamics and matrix interactions in the full range of mesoporous materials that can be prepared. This paper deals specifically with materials that have not previously been studied by single molecule methods: surfactant-containing and calcined mesoporous thin films of hexagonal order. The results show there is clear temporal heterogeneity in the mobilities of Nile Red molecules found within these films. Frequent, reversible adsorption of the dye to the surfactant−silica interface is noted in both surfactant-containing materials and those that have been calcined, reloaded with dye, and rehydrated by exposure to humid environments.

* Address correspondence to these authors. E-mail: higgins@ksu.edu and mmcollinson@vcu.edu.

‡ Current address: Department of Biochemistry & Molecular Biology, University of Maryland, 725 West Lombard Street, Baltimore, MD 21201.

† Current address: Department of Chemistry, Virginia Commonwealth University, 1001 W. Main St., Richmond, VA 23284.

10.1021/jp054178p CCC: $33.50
Published on Web 04/18/2006

This behavior contrasts with that of Nile Red reloaded into dry calcined films, for which the molecules are permanently adsorbed or otherwise entrapped at fixed locations.

Experimental Section

Sample Preparation. Silica sols were prepared by mixing tetramethoxysilane (TMOS, 0.5 mL), water (0.24 mL), absolute ethanol (1.57 mL), and HCl (0.10 mL of 0.1 M HCl) in a small vial. The sol was stirred for 1 h after addition of the above components and was then allowed to sit for an additional 24 h at room temperature. Cetyltrimethylammonium bromide (CTAB, 0.24 g) was then dissolved in the solution by vigorous stirring for 1 h. The final molar ratio for the silicate composites was typically 1:5.6:8:0.003:0.2 for TMOS:H_2O:ethanol:HCl:CTAB. For the preparation of dye-doped mesoporous films, a methanolic solution of Nile Red (Aldrich) was added to a portion of the above sol to yield a total dye concentration of 0.5 nM. Immediately after addition of the dye, ≈65 μL of the sol was spin cast (30 s at 6000 rpm) onto a clean glass coverslip (Fisher Premium). Transparent films of ≈1 μm thickness were obtained. The films were dried overnight at room temperature in a desiccator prior to use. Films studied without further treatment (see below) are referred to as "as-synthesized" films throughout this paper. FTIR spectra of these films indicate they contain small amounts of water (see the Supporting Information).

Surfactant-free mesoporous silica films were obtained with a similar procedure, followed by calcination of the films in a furnace. In this process, the films were first heated at 160 °C for 90 min. The temperature was then slowly increased (1 °C/min) to 350 °C, where it was held for 5 h. The calcined films were subsequently treated in an air plasma (Harrick Plasma) for 2−3 min to remove residual luminescent impurities that otherwise yielded significant background in the single molecule experiments. The calcined, plasma-treated films were then reloaded with dye by soaking them in 2 nM methanolic solutions of Nile Red for 1 h, followed by rinsing with ethanol to remove loosely bound dye. These films were also dried in a desiccator overnight before use.

Two different types of calcined-reloaded samples were studied by single molecule methods. Dry calcined films were maintained in a dry environment (dry air, 20% RH) throughout the recording of images and time transients, as described below. The dry calcined films incorporated little if any water, as deduced from their FTIR spectra (see the Supporting Information). Rehydrated calcined films (i.e., incorporating water within the mesopores) were stored in a humid environment (humidified air, 50% RH) for approximately 12 h prior to use. They were maintained under the same humid atmosphere throughout data collection. FTIR spectra of these films indicate they contain relatively less water than the as-synthesized films but more than the dry calcined films, although quantitative conclusions cannot be drawn.

Instrumentation. X-ray diffraction (XRD) was performed on a Bruker D8-Advance diffractometer with Cu Kα radiation (40 kV, 40 mA) at 1.54 Å with a 0.04° step size and a 15 s step time.

All single molecule and FCS experiments were conducted on a home-built sample scanning confocal microscope described previously.[40,41] Briefly, this system is built on an inverted epi-illumination microscope (Nikon TE-200). Light from a green helium−neon laser (543 nm) was used as the excitation source. A dichroic beam splitter (Chroma 565DCLP) was used to reflect the laser light into the back aperture of an oil immersion objective (Nikon Plan Fluor, 1.3 numerical aperture, 100× magnification). This objective was used both for focusing the excitation light into the sample and for collecting the resulting single molecule fluorescence. This system forms a nearly diffraction limited focus of ≈300 nm 1/e^2 radius in the sample. The incident laser power was maintained in the 200−400 nW range. Fluorescence collected from the sample was isolated from the excitation light by passage back through the dichroic beam splitter, a holographic notch filter, and a 100 nm wide bandpass filter centered at 650 nm. A single photon counting avalanche photodiode (EG&G) was used as the detector.

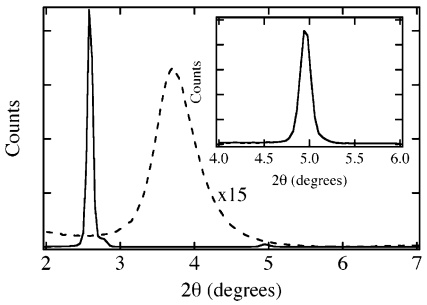

Figure 1. Small-angle X-ray diffraction data for the as-synthesized (—) and dry calcined (- - -) mesoporous silica thin films. The intensity of the broad peak from the calcined sample has been increased 15-fold. The inset depicts the (200) peak from the as-synthesized sample.

Fluorescence images were acquired by raster scanning the sample above the focused laser spot. The fluorescence signal was integrated for 40 ms per pixel in the 100 pixel × 100 pixel images. Single-point fluorescence time transients were obtained by positioning selected sample regions in the laser focus and recording the spectrally integrated fluorescence in time. Individual transients were recorded for up to 3 h, with a typical dwell time of 80 ms.

Simulations. Simulated time transients[42] and fluorescence images were employed to help interpret the experimental time transients and images.[43] In these studies, simulated data were numerically generated for perfectly homogeneous samples. Molecules were positioned randomly in a 30 × 30 μm^2 region with an areal density near 0.5 molecules/μm^2. The exact parameters used in each simulation are defined in the individual instances where such data are used (see below). The number of molecules present in the region was kept constant by having molecules that diffuse out of one edge of the region "wrap around" to reenter on the opposite side. During each time slice, Δt, each molecule was displaced from its previous position by a step of random size. The step size probability distribution was a Gaussian with a mean-square width of $2D\Delta t$ in each of the two dimensions simulated (in the sample plane). All molecules were assigned the same D value. This value was varied somewhat, as defined below, but was nominally held near 2×10^{-10} cm^2/s, consistent with experimental results. The Gaussian excitation spot was positioned at the center of the 30 × 30 μm^2 region and had a variance, s^2, of 2.3×10^{-10} cm^2. The maximum signal from each single molecule was set to 200 counts per data point. Signal variations due to rotational motions were not included in the simulations. Background equivalent to 20% of the signal was added to each transient. Random variations were also added to the signal and background counts to simulate the effects of shot noise. Time transients obtained in this manner were then treated identically to the experimental data.

Results and Discussion

X-ray Diffraction. Figure 1 shows typical XRD patterns obtained from the mesoporous films before and after calcination. The XRD pattern of the as-synthesized (i.e., surfactant-contain-

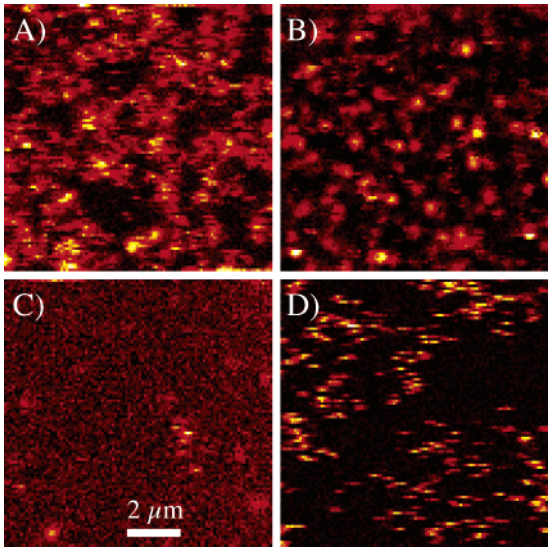

Figure 2. Fluorescence images of 10 × 10 μm^2 sample regions recorded for (A) as-synthesized mesoporous silica containing Nile Red at sub-nanomolar concentrations, (B) a dry calcined mesoporous film (imaged at 20% RH) also containing Nile Red in low concentrations, and (C) a blank image recorded for a calcined film, absent Nile Red. The calcined film was reloaded by immersing in a 2 nM methanolic Nile Red solution for 1 h, followed by rinsing in ethanol. (D) Simulated image obtained assuming an areal molecular density of 0.5 molecules/μm^2, with each molecule having a diffusion coefficient of 2×10^{-10} cm^2/s.

ing) silica film is most consistent with a hexagonal structure, having characteristic (100) and (200) peaks at $2\theta = 2.59°$ and 4.96°, respectively. These results yield a d spacing of $\approx 35 \pm 0.5$ Å. The absence of the (110) diffraction peak (expected at $2\theta = 4.41°$) indicates that the channels run parallel to the substrate surface.[6] Two smaller peaks observed in the $2\theta = 2-4°$ region likely indicate the films also incorporate some features of 3D hexagonal or cubic symmetries. XRD data obtained after removal of the CTAB by calcination (i.e., in the dry films) exhibit a less intense, broad, single peak at $2\theta = 3.70°$, corresponding to a d spacing of 23.9 Å (see Figure 1). These results reflect a 30% contraction and possible disordering of the mesoporous structure during calcination. Little or no change in the film structure is observed upon rehydration at 50% RH (data not shown). Neither addition of Nile Red to the sol nor its addition to the calcined films cause observable changes in any of these structures.

Images. Typical 10 × 10 μm^2 fluorescence images recorded for an as-synthesized mesoporous film doped with Nile Red and a dry calcined film reloaded with Nile Red are shown in Figure 2A,B. An image obtained from an undoped, calcined film is also shown for comparison (Figure 2C), as is a simulated image (Figure 2D). Images such as those shown in Figure 2A,B are most frequently used to locate single molecules and specific sample regions for further analysis. However, they also give initial, qualitative information on the molecular scale properties of the films. Images obtained from the as-synthesized films incorporate a few bright round fluorescent spots of diffraction-limited size, but are dominated by the many "streaks" that appear. These image streaks are reflective of line-by-line variations in the single molecule emission. Images recorded (not shown) for rehydrated calcined films imaged at 50% RH were virtually indistinguishable from those of the as-synthesized films and were also dominated by "streaks". In contrast, the dry (imaged at 20% RH) calcined films show predominantly round fluorescent spots (having Gaussian intensity profiles), with relatively few fluctuations occurring on a time scale similar to the image pixel time. Bulk FTIR spectra of these films show that the as-synthesized films contain the most water, followed by the rehydrated calcined films, while the dry calcined films incorporate little or none.

The bright round image spots in the dry calcined films are attributable to fluorescence from single molecules entrapped at fixed positions, whereas the streaks arise from temporal variations in the single molecule excitation and/or emission rates.[40,41,43] These temporal variations could result from translational and rotational diffusion,[44] spectral diffusion,[45] triplet blinking,[46] and/or variations in the quantum yield due to the formation of a nonfluorescent twisted internal charge transfer (TICT) state. The TICT state in Nile Red forms most readily in polar media.[40,41,47]

The relative numbers of "spots" and "streaks" observed in a given image have been shown previously to depend on the presence of residual solvents and the exact procedures used in film drying.[40,41,43,47,48] It has also been shown that certain dye-doped organically modified silicate films exhibit significant image streaking due to rapid molecular diffusion through fluid-filled environments found within these films.[41,43] It was concluded that the fluid-filled domains were comprised of liquidlike organosilicate oligomers.

In the present studies, the hydrated surfactant assemblies of the as-synthesized films and the "water-filled" pores of the rehydrated calcined samples are believed to behave as the "fluid-filled" domains, facilitating translational (and rotational) diffusion (see below). Comparison of the experimental and simulated fluorescence images shown in parts A and D of Figure 2 reveals that they are qualitatively similar, indicating translational diffusion could indeed be the root cause of the image streaks. The simulated image shown was obtained as described above, assuming a molecular density of 0.5 molecules/μm^2, with each molecule having a diffusion coefficient of 2×10^{-10} cm^2/s. The pixel time and simulated "scan rate" were identical with those used in the recording of the experimental data.

It is noteworthy that some streaks appear even in images of the dry calcined samples, and that some round spots are found in images otherwise dominated by streaks. In the dry calcined samples, many such fluorescence fluctuations can be attributed to triplet blinking[46] and possible quantum yield fluctuations due to intermittent formation of the TICT state.[40,41,47] The round spots observed in the as-synthesized films are due to molecules entrapped at fixed locations on the imaging time scale. Such spots do not appear in the simulated images (Figure 2D), suggestive of either substantial heterogeneity in the diffusion coefficient for different film regions or momentary adsorption of the diffusing species to the silica surface. Distinction between these two mechanisms can only be made by the recording and analysis of time transients, as described below.

Time Transients. Spectrally integrated fluorescence time transients were recorded for numerous different films and different locations within each of the three classes of films. Figure 3 shows a representative fluorescence time transient for Nile Red dispersed within an as-synthesized film (Figure 3A), a simulated time transient (Figure 3B) for diffusing molecules (0.6 molecules/μm^2, $D = 3 \times 10^{-10}$ cm^2/s), and a time transient obtained from a particularly long-lived molecule in a dry calcined sample (Figure 3D). Transients obtained from rehydrated calcined samples studied at 50% RH were similar in appearance to those obtained from the as-synthesized films.

The experimental time transients from the as-synthesized and rehydrated calcined samples (as well as the simulated transients)

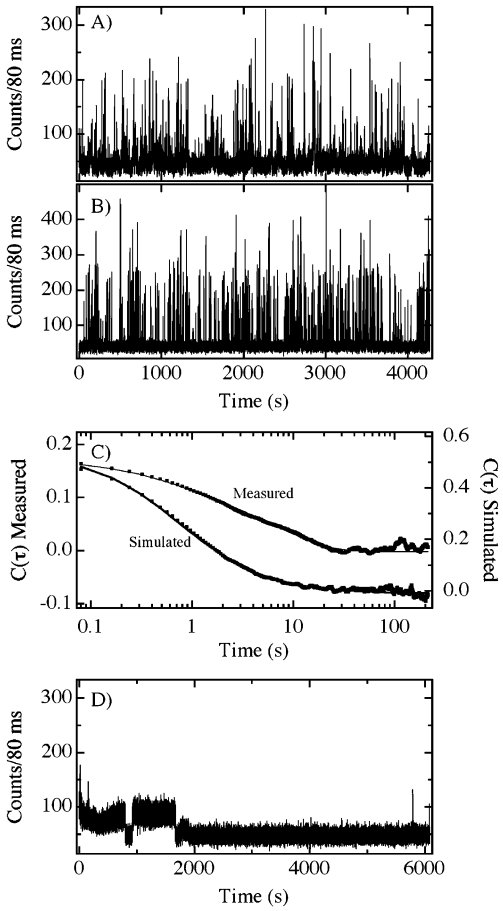

Figure 3. (A) Representative fluorescence time transient recorded for Nile Red in an as-synthesized mesoporous silica film. (B) Simulated time transient obtained by using a molecular areal density of 0.6 molecules/μm^2 and $D = 3 \times 10^{-10}$cm^2/s. (C) Autocorrelations (points) and fits (lines) to eq 2 for the data shown in parts A and B. (D) Fluorescence transient recorded for a long-lived Nile Red molecule in a dry calcined sample.

exhibit short bursts of fluorescence separated by periods over which only background counts are observed. Importantly, these bursts continue to occur even for extremely long transients, indicating they arise from the translational diffusion of different Nile Red molecules (one at a time) in to and out of the excitation/detection volume. Such behavior is very similar to that found in solution-phase FCS studies of single molecule diffusion.[33,49] We have also observed similar behavior for single molecules trapped in "disordered" (and organically modified) sol−gel derived silicate films.[40,41,43] Finally, several publications on mass transport in ordered and disordered silica materials have also reported similar observations.[34−36,38,39,50]

The time transients for the fixed spots observed in the dry calcined samples exhibit markedly different behavior. The fluorescence in such transients is typically constant (aside from shot noise fluctuations), ending in a permanent, discrete drop in the fluorescence to background. Most importantly, few if any fluorescence bursts are ever observed, consistent with the detection of a single, immobile molecule in each time transient. The representative transient shown in Figure 3D exhibits slow variations over time and a single reversible "blinking" event, prior to permanent photobleaching after about 30 min of continuous illumination. Nile Red molecules most commonly bleach within a few tens of seconds, indicating that this particular molecule may have been confined to a collapsed pore, deep within the film.

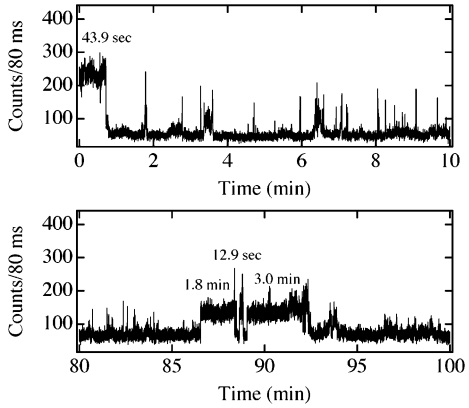

Figure 4. Expanded sections of representative time transients showing long-term adsorption events in an as-synthesized film. Each of the four designated events is labeled with the measured desorption time. Two additional features at ≈3.5 and 6.5 min in the top transient do not exhibit constant signal levels and therefore are believed to be due to diffusional processes rather than adsorption.

While the time transients for the as-synthesized and rehydrated calcined samples most commonly exhibit the relatively short bursts expected for simple translational diffusion of the molecules, behavior similar to that observed in the dry calcined samples is also sometimes observed. Specifically, the signal sometimes abruptly stops fluctuating and becomes approximately constant, aside from shot-noise variations. Figure 4 depicts expanded sections of two time transients in which the fluorescence remained constant for relatively long periods. Several such events are labeled with the time over which the signal remained approximately constant (and above background). As in the literature,[34,42,50] such events are attributed to adsorption of the individual molecules at fixed locations within the film. Previous studies of monolithic mesoporous materials[36,38] and disordered mesoporous films[39] have also yielded indirect evidence of dye adsorption, supporting this assignment. Adsorption events can end in desorption of the molecule and resumption of its diffusive motions. However, particularly long events often appear to end in permanent photobleaching. It should be noted that adsorption events on the order of a minute or longer (as in Figure 4) are believed to represent only the longest such events and shorter adsorption events are very likely present as well (see below); they are simply not as obvious.

While it is possible that very rare diffusive events could yield long periods where the signal remains above background, the simulations prove this is not the case for the particularly long events observed here. Adsorption phenomena were explicitly excluded from the simulations. Therefore, the longest events observed in the simulations depict the longest possible rare diffusive events. The longest such events observed in approximately 30 simulated transients having $D = (1-3) \times 10^{-10}$ cm^2/s were ≈25 s in length, and these were extremely rare (i.e., less than one such event on average in individual transients 3 h in length). More importantly, the signal appearance in such events was qualitatively different from that observed experimentally. Specifically, the signal continued to fluctuate during the simulated events, while it remains approximately constant during real events observed experimentally. Therefore, it is concluded that the long transit-time events observed experimentally are actually due to periodic, reversible adsorption of Nile Red to the silica surfaces.

Autocorrelation of the fluorescence time transients provides a means to quantitatively measure both the rate of molecular diffusion and the representative time scales for molecular

adsorption. Such analyses also provide a means to assess the relative importance of adsorption events in each transient. Here, the normalized autocorrelation function, $C(\tau)$, for each transient is calculated as follows:

$$C(\tau) = \frac{\langle i(t)i(t+\tau)\rangle}{\langle i(t)\rangle^2} - 1 \qquad (1)$$

Autocorrelations of the experimental and simulated data shown in Figure 3A,B are given in Figure 3C.

The autocorrelated data were fit to an appropriate model[34−36,50] selected for its inclusion of both two-dimensional diffusion (within the film plane) and surface adsorption of the Nile Red molecules. The data reported herein were fit as follows:

$$C(\tau) = \frac{A_d}{(1 + D\tau/s^2)} + A_a \exp(-\tau k) \qquad (2)$$

Representative fits of the autocorrelation data using eq 2 are also shown in Figure 3C. In eq 2, A_d and A_a are the amplitudes of the diffusion and adsorption components of the decay, respectively. D is the diffusion coefficient for Nile Red, s^2 is the beam variance (2.3×10^{-10} cm^2), and k is the rate constant for desorption of adsorbed species. The value for s^2 was obtained by autocorrelating the fluorescence images acquired from calcined samples and fitting the resulting curves to Gaussian profiles, as described previously.[43]

Of the 79 experimental time transients collected from the as-synthesized samples and analyzed by this procedure, only three could be fit satisfactorily with A_a set to zero (i.e., no detectable adsorption events occurred in these three transients). All others required both the diffusional and exponential terms to properly fit the data. In contrast, only 5% (at most) of the autocorrelations derived from simulated time transients could not be fit by using the diffusional component alone in eq 2. These results indicate that inclusion of the second decay component in the majority of the experimental autocorrelations does not arise from uncertainties in the analysis. Rather, it reflects the presence of real signal variations (i.e., due to adsorption) occurring on a different time scale than diffusion.

Figure 5 depicts histograms of the diffusion coefficients and desorption rate constants obtained by fitting all 79 autocorrelations. From these data, an average D of $2.4(\pm0.8) \times 10^{-10}$ cm^2/s (error bars indicate the 95% confidence interval) is obtained for Nile Red in the as-synthesized mesoporous films. Fitting of the histogram in Figure 5A to a Gaussian function yields a value for the most common D of 1.1×10^{-10} cm^2/s. Likewise, average and most common values for k are determined to be 0.040 and 0.037 s^{-1}, respectively, consistent with a characteristic mean desorption time of $25(\pm9)$ s. Similarly, an average D of $2.6(\pm1.0) \times 10^{-10}$ cm^2/s and a mean desorption time of $40(\pm10)$ s are obtained from the rehydrated calcined samples. Note that the mean desorption times reflect the average length of time the molecules spend adsorbed to the silica surface, while the simulated time transients yielded only very few rare diffusive events of this same length.

The widths of the D and k distributions shown in Figure 5 are believed to be due almost entirely to errors associated with fitting the autocorrelation data.[43] They do not appear to reflect a significant level of heterogeneity in either diffusional or adsorption/desorption processes. This conclusion is consistent with sample heterogeneity occurring over length scales much smaller than the diffraction limited focus of the microscope.

The above results show that the rates of Nile Red diffusion observed in the as-synthesized and rehydrated calcined films

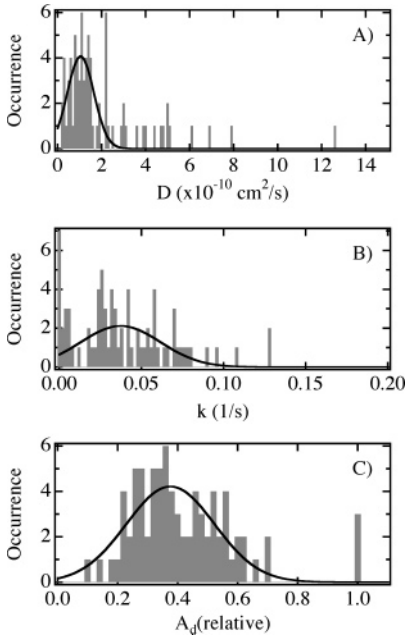

Figure 5. Histograms showing the distributions of measured D values (A), k values (B), and amplitudes (C) of the diffusional component of the autocorrelation decays relative to total decay amplitude for as-synthesized samples.

are indistinguishable. The similarity in diffusion coefficients indicates that water present within the mesopores and/or associated with the surfactant mesophase in the as-synthesized materials plays an important role in determining the mobility of the Nile Red molecules. The fact that water is present in both the as-synthesized and rehydrated calcined films suggests water may be the dominant factor. However, because the pore sizes and organization are significantly different before and after calcination, the exact extent to which surfactant, water, pore size, and pore order control molecular mobility remains uncertain.

The mean desorption times in the as-synthesized and rehydrated calcined films do, however, differ at better than the 80% confidence level. Specifically, Nile Red molecules in the rehydrated samples spend longer times (on average) adsorbed to the silica surface, relative to those in the as-synthesized films. While this effect may be biased by photobleaching of the adsorbed molecules, these results suggest that desorption of the Nile Red molecules into the surfactant phase of the as-synthesized materials is more favorable than desorption into the "water-filled" pores of the rehydrated calcined materials. Such an effect is consistent with the known hydrophobicity and solubility properties of Nile Red.

Figure 5 also depicts a histogram showing the apparent relative contributions of diffusion and adsorption to the autocorrelation decays for the as-synthesized samples. Here, A_d has been normalized to the total amplitude of the decay as follows:

$$A_d(\text{relative}) = \frac{A_d}{A_d + A_a} \qquad (3)$$

An average relative A_d of $0.43(\pm0.04)$ is obtained for the as-synthesized films, along with an average relative A_a of $0.57(\pm0.04)$. For the rehydrated calcined samples, similar results are obtained with $A_d = 0.6(\pm0.1)$ and $A_a = 0.4(\pm0.1)$. These results indicate that a significant fraction of each autocorrelation decay arises from reversible adsorption events in both the as-synthesized and rehydrated calcined samples. However, the

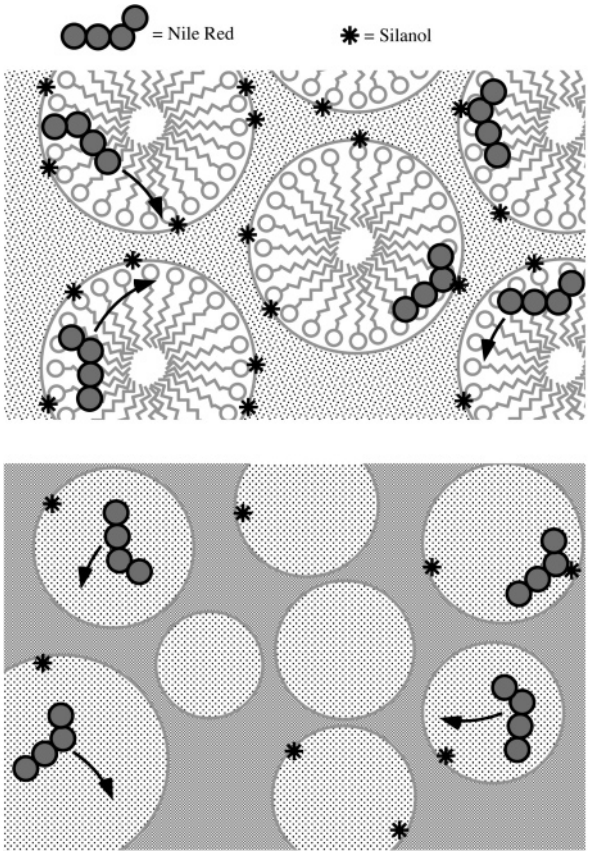

Figure 6. Model for diffusion and adsorption of Nile Red within the as-synthesized (top) and rehydrated calcined (bottom) films. The dye moves relatively freely through the surfactant-filled and/or hydrated pores, periodically encountering surface silanols (stars) on the silica pore surfaces to which it can hydrogen bond, leading to reversible adsorption events.

frequency of adsorption is clearly different, with the A_d (and A_a) values differing at better than the 95% confidence level between the two samples.

The autocorrelation decays appear to be dominated by adsorption phenomena in the case of the as-synthesized samples and by diffusing molecules in the case of the rehydrated calcined samples. Taken together, the results for the autocorrelation decay amplitudes and mean desorption times indicate that while the Nile Red molecules adsorb less frequently to the silica surfaces in the rehydrated calcined samples, they adsorb for longer periods of time. Nile Red adsorption likely involves formation of a hydrogen bond between a surface silanol and the quinonal oxygen of Nile Red. Less frequent adsorption of Nile Red to the pore surfaces in the rehydrated calcined samples is consistent with a reduction in the concentration of surface silanols after calcination.

For the as-synthesized materials, it is concluded that the Nile Red molecules spend the majority of their time in the relatively polar regions of the surfactant mesophase, near the surfactant−silicate interface. The molecules are free to move about in this region and frequently encounter, adsorb, and desorb from the surface. The relatively high concentration of surface silanols produces frequent adsorption events. In the calcined samples, silanol condensation and collapse of the pores means that far fewer silanol sites are available for adsorption. Although mass transport is facilitated by water in the rehydrated films, dissolution of Nile Red in water is relatively less favorable than that in the surfactant phase and so the molecules spend more time adsorbed to the surface. Figure 6 shows a model for how the pores might appear in these two samples. Finally, in the dry films, the molecules are permanently adsorbed at fixed film sites.

Conclusions

In summary, single molecule imaging and fluorescence correlation spectroscopy have been employed to probe single molecule diffusion and surface adsorption in as-synthesized (i.e., surfactant-containing) mesoporous silica thin films and in calcined, plasma-treated mesoporous films. In the latter samples, both dry and rehydrated samples were investigated. The results obtained prove that Nile Red molecules move readily through the as-synthesized and rehydrated calcined materials, but that they also exhibit relatively frequent adsorption to fixed sites on the silica pore surfaces. Characteristic diffusion coefficients for the Nile Red molecules are $\approx 2 \times 10^{-10}$ cm^2/s. The average adsorbed molecule in the as-synthesized samples spends ≈25 s attached to the silica surface before it desorbs or undergoes irreversible photobleaching. In the rehydrated calcined films, the average molecule spends a relatively longer 40 s in the adsorbed state, although adsorption occurs somewhat less frequently. In stark contrast, the Nile Red molecules appear to be completely immobile in the dry calcined films. The results indicate that the surfactant phases of the as-synthesized materials and the hydrated pores of calcined materials exposed to high humidity environments behave as fluid-filled domains that greatly facilitate mass transport of the dye. The results of these studies provide valuable new information on the rates of mass transport and surface adsorption events of most relevance to applications of these and other mesoporous materials in chemical separations, sensing, and optical device applications.

Acknowledgment. The authors gratefully acknowledge the support of the National Science Foundation (CHE-0316466) in these studies. Bei Liu is thanked for helpful discussions on the interpretation of the XRD data.

Supporting Information Available: FTIR spectra of the as-synthesized and calcined films. This material is available free of charge via the Internet at http://pubs.acs.org.

References and Notes

(1) Kresge, C. T.; Leonowicz, M. E.; Roth, W. J.; Vartuli, J. C.; Beck, J. S. *Nature* **1992**, *359*, 710−712.

(2) Beck, J. S.; Vartuli, J. C.; Roth, W. J.; Leonowicz, M. E.; Kresge, C. T.; Schmitt, K. D.; Chu, C. T.-W.; Olson, D. H.; Sheppard, E. W.; McCullen, S. B.; Higgins, J. B.; Schlenker, J. L. *J. Am. Chem. Soc.* **1992**, *114*, 10834−10843.

(3) Tolbert, S. H.; Schäffer, T. E.; Feng, J.; Hansma, P. K.; Stucky, G. D. *Chem. Mater.* **1997**, *9*, 1962−1967.

(4) Yang, H.; Kuperman, A.; Coombs, N.; Mamiche-Afara, S.; Ozin, G. A. *Nature* **1996**, *379*, 703−705.

(5) Yang, H.; Coombs, N.; Sakolov, I.; Ozin, G. A. *Nature* **1996**, *381*, 589−592.

(6) Alberius, P. C. A.; Frindell, K. L.; Hayward, R. C.; Kramer, E. J.; Stucky, G. D.; Chmelka, B. F. *Chem.* Mater. **2002**, *14*, 3284−3294.

(7) Grosso, D.; Balkenende, A. R.; Albouy, P. A.; Lavergne, M.; Mazerolles, L.; Babonneau, F. *J. Mater. Chem.* **2000**, *10*, 2085−2089.

(8) Grosso, D.; Balkenende, A. R.; Albouy, P. A.; Ayral, A.; Amenitsch, H.; Babonneau, F. *Chem. Mater.* **2001**, *13*, 1848−1856.

(9) Hernandez, R.; Franville, A.-C.; Minoofar, P.; Dunn, B.; Zink, J. I. *J. Am. Chem. Soc.* **2001**, *123*, 1248−1249.

(10) Huang, M. H.; Dunn, B. S.; Soyez, H.; Zink, J. I. *Langmuir* **1998**, *14*, 7331−7333.

(11) Huang, M. H.; Soyez, H. M.; Dunn, B. S.; Zink, J. I. *Chem. Mater.* **2000**, *12*, 231−235.

(12) Zhao, D.; Yang, P.; Margolese, D. I.; Chmelka, B. F.; Stucky, G. D. *Chem. Commun.* **1998**, 2499−2500.

(13) Lu, Y.; Ganguli, R.; Drewien, C. A.; Anderson, M. T.; Brinker, C. J.; Gong, W.; Guo, Y.; Soyez, H.; Dunn, B.; Huang, M. H.; Zink, J. I. *Nature* **1997**, *389*, 364−368.

(14) Collinson, M. M. Structure, Chemistry, and Applications of Sol−Gel Derived Materials. In *Chalcogenide Glasses and Sol−Gel Materials*; Nalwa, H. S., Ed.; Academic Press: New York, 2001; Vol. 5, pp 163−194.

(15) Liu, N.; Assink, R. A.; Brinker, C. J. *Chem. Commun.* **2003**, 370−371.

(16) Liu, N.; Assink, R. A.; Smarsly, B.; Brinker, C. J. *Chem. Commun.* **2003**, 1146−1147.

(17) Wong, E. M.; Markowitz, M. A.; Qadri, S. B.; Golledge, S. L.; Castner, D. G.; Gaber, B. P. *Langmuir* **2002**, *18*, 972−974.

(18) Ferrer, M.; Lianos, P. *Langmuir* **1996**, *12*, 5620−5624.

(19) Ogawa, M. *Langmuir* **1995**, *11*, 4639−4641.

(20) Wirnsberger, G.; Scott, B. J.; Stucky, G. D. *Chem. Commun.* **2001**, 119−120.

(21) Bae, J. Y.; Jung, J.-I.; Bae, B.-S. *J. Mater. Res.* **2004**, *19*, 2503−2509.

(22) Marlow, F.; McGehee, M. D.; Zhao, D.; Chmelka, B. F.; Stucky, G. D. *Adv. Mater.* **1999**, *11*, 632−636.

(23) Yang, P.; Wirnsberger, G.; Huang, H. C.; Cordero, S. R.; McGehee, M. D.; Scott, B.; Deng, T.; Whitesides, G. M.; Chmelka, B. F.; Buratto, S. K.; Stucky, G. D. *Science* **2000**, *287*, 465−467.

(24) Loerke, J.; Marlow, F. *Adv. Mater.* **2002**, *14*, 1745−1749.

(25) Keeling-Tucker, T.; Brennan, J. D. *Chem. Mater.* **2001**, *13*, 3331−3350.

(26) Huang, M. H.; Dunn, B. S.; Zink, J. I. *J. Am. Chem. Soc.* **2000**, *122*, 3739−3745.

(27) Minoofar, P. N.; Dunn, B. S.; Zink, J. I. *J. Am. Chem. Soc.* **2005**, *127*, 2656−2665.

(28) Minoofar, P. N.; Hernandez, R.; Chia, S.; Dunn, B.; Zink, J. I.; Franville, A.-C. *J. Am. Chem. Soc.* **2002**, *124*, 14388−14396.

(29) Moerner, W. E. *J. Phys. Chem. B* **2002**, *106*, 910−927.

(30) Tamarat, P.; Maali, A.; Lounis, B.; Orrit, M. *J. Phys. Chem. A* **2000**, *104*, 1−16.

(31) Higgins, D. A.; Hou, Y. Single Molecule Spectroscopy Studies to Characterize Nanomaterials. In *Encyclopedia of Nanoscience and Nanotechnology*; Schwartz, J. A., Contescu, C., Putyera, K., Eds.; Marcel-Dekker: New York, 2004; pp 3575−3596.

(32) Elson, E. L.; Magde, D. *Biopolymers* **1974**, *13*, 1−27.

(33) Shera, E. B.; Seitzinger, N. K.; Davis, L. M.; Keller, R. A.; Soper, S. A. *Chem. Phys. Lett.* **1990**, *174*, 553−557.

(34) Wirth, M. J.; Swinton, D. J. *Anal. Chem.* **1998**, *70*, 5264−5271.

(35) Zhong, Z.; Lowry, M.; Wang, G.; Geng, L. *Anal. Chem.* **2005**, *77*, 2303−2310.

(36) Mahurin, S. M.; Dai, S.; Barnes, M. D. *J. Phys. Chem. B* **2003**, *107*, 13336−13340.

(37) Schütz, G. J.; Schindler, H.; Schmidt, T. *Biophys. J.* **1997**, *73*, 1073−1080.

(38) Seebacher, C.; Hellriegel, C.; Deeg, F.-W.; Brauchle, C.; Altmaier, S.; Behrens, P.; Mullen, K. *J. Phys. Chem. B* **2002**, *106*, 5591−5595.

(39) McCain, K. S.; Hanley, D. C.; Harris, J. M. *Anal. Chem.* **2003**, *75*, 4351−4359.

(40) Bardo, A. M.; Collinson, M. M.; Higgins, D. A. *Chem. Mater.* **2001**, *13*, 2713−2721.

(41) Higgins, D. A.; Collinson, M. M.; Saroja, G.; Bardo, A. M. *Chem. Mater.* **2002**, *14*, 3734−3744.

(42) Wirth, M. J.; Ludes, M. D.; Swinton, D. J. *Appl. Spectrosc.* **2001**, *55*, 663−669.

(43) Martin-Brown, S. A.; Fu, Y.; Saroja, G.; Collinson, M. M.; Higgins, D. A. *Anal. Chem.* **2005**, *77*, 486-494.

(44) Gilliland, J. W.; Yokoyama, K.; Yip, W. T. *Chem. Mater.* **2004**, *16*, 3949−3954.

(45) Lu, H. P.; Xie, X. S. *Nature* **1997**, *385*, 143−146.

(46) Ha, T.; Enderle, T.; Chemla, D. S.; Selvin, P. R.; Weiss, S. *Chem. Phys. Lett.* **1997**, *271*, 1−5.

(47) Hou, Y.; Higgins, D. A. *J. Phys. Chem. B* **2002**, *106*, 10306−10315.

(48) Mei, E.; Bardo, A. M.; Collinson, M. M.; Higgins, D. A. *J. Phys. Chem. B* **2000**, *104*, 9973−9980.

(49) Nie, S.; Chiu, D. T.; Zare, R. N. *Science* **1994**, *266*, 1018−1021.

(50) Wirth, M. J.; Swinton, D. J. *J. Phys. Chem. B* **2001**, *105*, 1472−1477.